

Collimation of dense plasma jets created by low-energy laser pulses and studied with soft x-ray laser interferometry

Michael A. Purvis,¹ Jonathan Grava,¹ Jorge Filevich,¹ Duncan P. Ryan,² Stephen J. Moon,³ James Dunn,³
Vyacheslav N. Shlyaptsev,¹ and Jorge J. Rocca^{1,2}

¹*NSF ERC for Extreme Ultraviolet Science and Technology and Department of Electrical and Computer Engineering,
Colorado State University, Fort Collins, Colorado 80523, USA*

²*Department of Physics, Colorado State University, Fort Collins, Colorado 80523, USA*

³*Lawrence Livermore National Laboratory, Livermore, California 94551, USA*

(Received 23 December 2009; published 15 March 2010)

The physical mechanisms driving the collimation of dense plasma jets created by low-energy (~ 0.6 J) laser pulse irradiation of triangular grooves were studied for different target materials using soft-x-ray interferometry and hydrodynamic code simulations. The degree of collimation of jets created by irradiating C, Al, Cu, and Mo targets at intensities of $I=1 \times 10^{12}$ W cm⁻² with 120 ps laser pulses was observed to increase significantly with the atomic number. Radiation cooling is found to be the cause of the increased collimation, while the main effect of the increase in mass is to slow the jet evolution.

DOI: [10.1103/PhysRevE.81.036408](https://doi.org/10.1103/PhysRevE.81.036408)

PACS number(s): 52.50.Jm, 52.70.-m, 52.65.-y, 07.60.Ly

I. INTRODUCTION

The dynamics of high Mach number plasma jets is relevant to astrophysics and laboratory plasmas [1–3]. There is interest in understanding the jet formation and expansion dynamics, and in particular the physical mechanisms that maintain jet collimation. High-energy laser facilities including Nova [4], Gekko XII [5], and Omega [6] have been used to create highly collimated supersonic jets (Mach numbers between 3 and 50) by irradiating cone-shaped targets. High-energy laser pulses (0.5–6 kJ) from these lasers have created plasma jets in which radiation cooling significantly lowers the pressure in the jet, resulting in a dense highly collimated jet. Laboratory plasma jets in which plasma radiation has a major effect in the formation and collimation were also recently studied by laser irradiation of flat targets with 100 J laser pulses at the Prague Asterix Laser System laser facility [7–10]. In several of these experiments an increase in the atomic number (Z) of the target material was correlated with an increase in jet collimation [5,10]. High Mach number jets have also been produced using fast Z -pinch wire arrays [11,12]. Experimental techniques used to study the dynamics of these jets have included imaging [4–6,11–13], spectroscopy [12], backlighting [4–6,14], and optical interferometry [9–11,15]. In the case of optical interferometry probe beam refraction in regions of steep density gradients can be a significant limitation. The reduced refraction of a soft-x-ray probe allows mapping of the electron density in the plasma regions of significantly higher density gradients [16–18]. This motivates the use of soft-x-ray laser interferometry to probe dense plasma laboratory jets.

We have recently produced planar Al plasma jets by laser irradiation of 1-mm-long 90° triangular grooved cavities with low-energy laser pulses of ~ 0.6 J [19]. Soft-x-ray laser interferometry yielded electron-density maps that revealed the formation of thin plasma jets that expand with a Mach number of 3–5 with plasma densities in excess of $\sim 1 \times 10^{20}$ cm⁻³. The jet formation is initiated by material ablated near the target vertex that expands along the symmetry

plane. The jets are augmented by the continual sequential arrival of wall material to the symmetry plane where it collides and is redirected outward [19]. Simulations performed with the radiation hydrodynamics code HYDRA revealed that these jets are in the radiatively coupled regime in which radiation cooling is comparable to adiabatic cooling. In this paper we present results of the study of the physical mechanisms that affect the collimation of plasma jets generated irradiating a broad range of target materials: carbon, aluminum, copper, and molybdenum ($Z=6, 13, 29,$ and $42,$ respectively) with low-energy (<1 J) optical laser pulses.

II. EXPERIMENTAL PROCEDURE

The plasma jets were formed by irradiation of 90° triangular grooves with Ti:sapphire laser pulses ($\lambda=800$ nm) of ~ 0.6 J energy and 120 ps duration. The laser beam was shaped to create a $350 \mu\text{m} \times 1.8$ mm line focus onto the target with an intensity of $\sim 10^{12}$ W cm⁻². The targets were machined to produce 500- μm -wide 250- μm -deep grooves along the 1 mm target width. Multiple grooves were machined in one target with a separation of 1 mm to allow for the rapid acquisition of multiple measurements. The depth variation from one groove to another was less than $\pm 20 \mu\text{m}$. The grooves in the carbon target were cut with the same angle but with a slightly larger depth ($\sim 320 \mu\text{m}$) than those in the other materials. Nevertheless, because the jet is mainly formed at the bottom 200 μm of the groove, the jet evolution is not significantly influenced by this difference in groove depth.

Sequences of interferograms were obtained using a Mach-Zehnder interferometer based on diffraction gratings [17,18]. The interferometer is designed to operate at the $\lambda=46.9$ nm wavelength of a compact Ne-like Ar capillary discharge-pumped soft-x-ray laser [20,21]. In the configuration used here the laser emits pulses of ~ 1.2 ns duration and ~ 0.15 mJ of energy [21] with good spatial coherence [22]. The short wavelength of the laser reduces beam refraction in sharp electron-density gradients present in the plasma, allow-

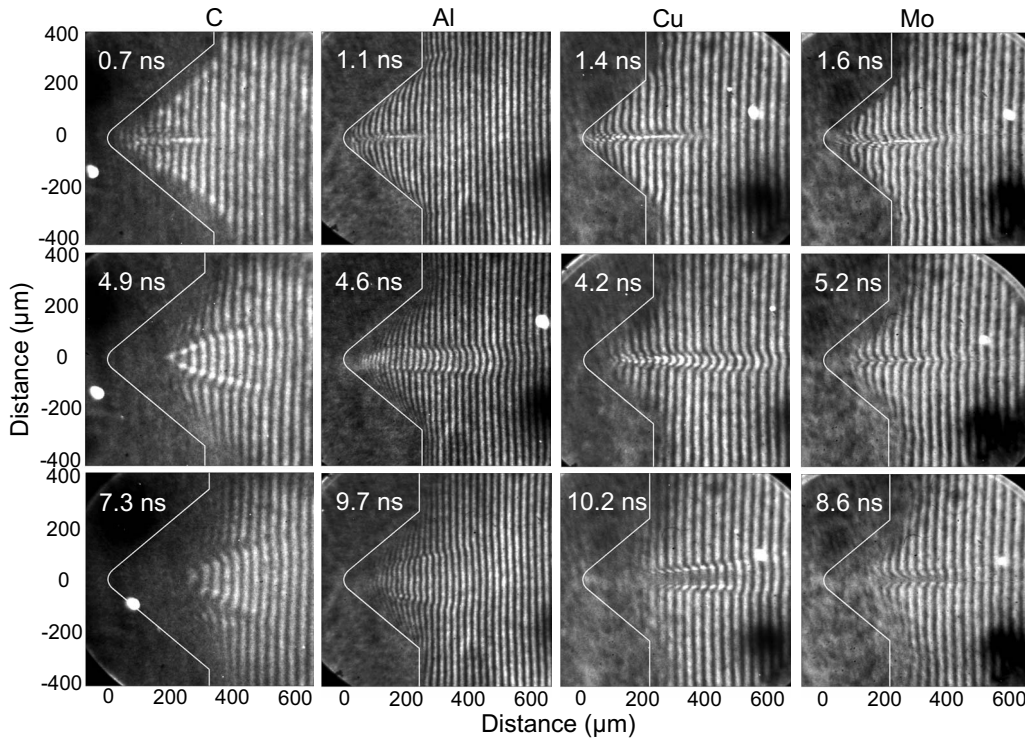


FIG. 1. Sequences of soft-x-ray laser interferograms of plasma jets created by laser irradiation of C, Al, Cu, and Mo targets at intensities of $\sim 10^{12}$ W cm $^{-2}$. The times are measured with respect to the beginning of the 120 ps laser heating pulse. The position of the target surface is represented by the white line. Jet collimation is observed to increase for the higher Z targets.

ing the probing of significantly higher densities than possible with optical lasers [16]. A multilayer coated Si/Sc spherical mirror ($R=30$ cm) with $\sim 40\%$ reflectivity [23] is used to image the plasma onto a charge-coupled device detector with $25\times$ magnification [17]. A more detailed description of the soft-x-ray laser interferometry setup used in the experiment is given in a previous publication [19].

III. EXPERIMENTAL RESULTS

Figure 1 displays sequences of interferograms that map the evolution of jets created by irradiating targets of each of the four materials. The time indicated is measured from the beginning of the 120 ps heating laser pulse to the peak of the soft-x-ray laser probe pulse. The first row of interferograms, corresponding to times of 0.7–1.6 ns, shows a narrow and elongated region with a high number of fringe shifts along the symmetry plane of the target. The interference fringes in this region are locally scrambled by strong refraction of the probe beam in the high-density gradients present. This denotes the presence of a high-density plasma jet with a high length-to-width ratio that in the case of the heaviest element, Mo, exceeds 20. The second row of interferograms, which correspond to times between 4.2 and 5.2 ns after laser irradiation, shows that the steep density gradients have relaxed, allowing for more fringes to be resolved within the jet. The interferograms show noticeable differences in the jet width for the different target materials. The jets created from the lower Z target materials (C and Al) display significant lateral expansion, while the higher Z jets (Cu and Mo) remain

highly collimated and narrow. The last row of interferograms (7.3–10.2 ns) corresponds to times at which the plasma has significantly cooled. These images show absorption of the probe beam near the target walls and also within the high Z jets due to the photoionization of low charge ions by the 26.5 eV photons, preventing the observation of fringes in those regions. Nevertheless, a measurement of the jet's width and length can still be inferred, which shows that the higher Z plasmas are considerably more collimated.

Figure 2 shows electron-density maps obtained from the analysis of the interferograms in Fig. 1. The interferograms were analyzed assuming that the plasma is uniform along the direction of the probe beam, and that only the free electrons contribute to the index of refraction. The first approximation is justified by the relatively small expansion of the plasma in the direction parallel to the probe beam [24]. The free-electron approximation was verified by atomic calculations which show that the contribution of bound electrons to the indices of refraction of the Al, Cu, and Mo plasmas is negligible at this wavelength [25]. However, we have previously shown that this assumption is not valid for C plasmas probed with 46.9 nm light when significant densities of low charge ions (CI–CIII) are present [24–26]. Nevertheless, if the degree of ionization is such that the concentration of those ions is sufficiently low, the bound-electron contribution to the index of refraction can be neglected and an index dependent only on the free-electron density can be used to obtain direct electron-density measurements [24]. The simulations discussed in the next section indicate that within the C jet stream the mean degree of ionization during the first 5 ns is

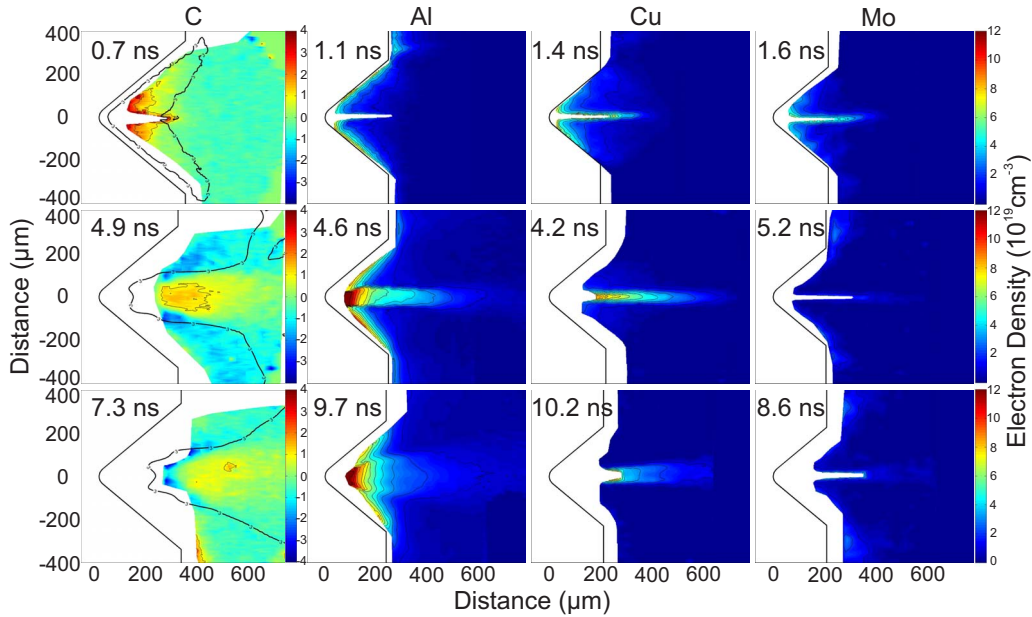


FIG. 2. (Color online) Electron-density maps for C, Al, Cu, and Mo obtained from the interferograms in Fig. 1. Regions in which the density could not be measured due to probe beam refraction are colored white. In the case of carbon the free-electron approximation is computed to be valid in the region to the right of the black line.

4–6, justifying the electron-density measurements within the jet region.

The measured electron densities within the Al jet exceed $1.3 \times 10^{20} \text{ cm}^{-3}$ at distances of 100–125 μm from the target vertex in the 4.6 ns frame. Also, since the density is also measured to decrease monotonically along the jet length, it can be expected to be larger near the target vertex. There is at least an order of magnitude in electron-density contrast between the plasma in the jet and the surrounding plasma. A comparison of the densities between the different materials shows that the lower Z jets are generally less dense. This trend is illustrated by the last row of density maps, which reveals a wider carbon plasma with densities of $\sim 1 \times 10^{19} \text{ cm}^{-3}$ measured at a distance of $\sim 300 \mu\text{m}$ from the target vertex. Comparatively, the Al and Cu jets reach densities of 3×10^{19} and $5 \times 10^{19} \text{ cm}^{-3}$, respectively, at this location. The density of the Mo jet is not measurable due to absorption of the probe beam.

IV. SIMULATIONS AND DISCUSSION

To aid the understanding of the physical mechanisms that shape the jets, two-dimensional numerical simulations were performed using the single fluid hydrodynamics code HYDRA [27,28]. Plasma discretization was accomplished by employing an arbitrary Lagrangian-Eulerian mesh. Up to 5000 rays with randomly distributed energies were used to simulate the heating beam. The laser energy was assumed to be deposited through inverse bremsstrahlung absorption, which dominates laser absorption at these intensities. The Livermore equation of state was used throughout the calculations. Radiation transport was treated using the technique of multigroup radiation diffusion. Calculations were performed assuming local thermal equilibrium (LTE). In selected cases non-local

thermal equilibrium calculations were also performed to verify that the results do not differ significantly from those presented using the LTE version.

The code operated in this manner reproduces well the measured electron-density maps shown in Fig. 2, and in particular the observed differences in jet collimation. Figure 3 shows the results of simulations for the C, Al, and Cu plasmas. The simulations show that the jet expands along the symmetry plane reaching supersonic velocities ($M \sim 7-10$ in the case of Cu). The experiment agrees with simulations in showing that the velocity increases as a function of distance from the target (i.e., the lower densities at the tip of the jet expand at a higher velocity). For jets of different Z , during

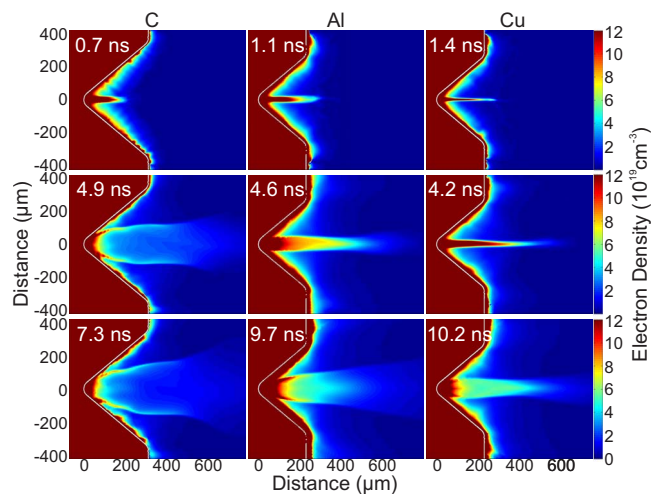


FIG. 3. (Color online) Simulated electron-density maps for C, Al, and Cu plasma jets at different times during the evolution. The irradiation conditions are assumed to be those used to obtain the interferograms in Fig. 1.

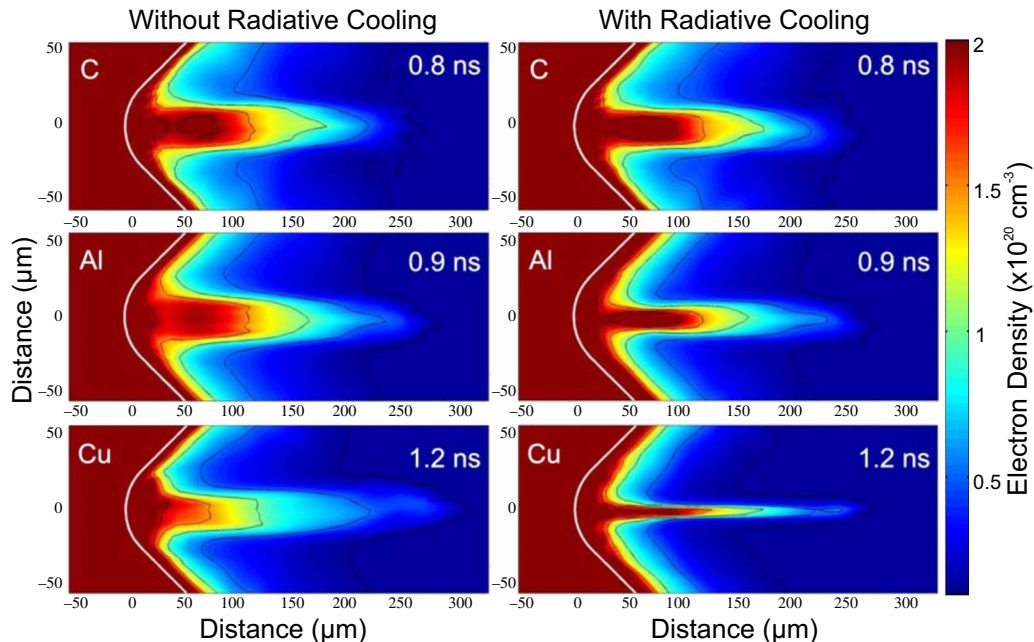


FIG. 4. (Color online) Computed electron-density distribution resulting from simulations with (right column) and without (left column) radiation cooling for C, Al, and Cu plasma jets. The times were selected to allow for jets of similar length. In the absence of radiation cooling a similar degree of collimation is computed for jets of the same length. Radiation cooling increases the collimation of the higher Z jets.

the first stages of jet evolution, the velocity corresponding to regions of equal density decreases with increasing target atomic mass. For example, at 1 ns in the plasma evolution the jet region with a density of $1 \times 10^{19} \text{ cm}^{-3}$ expands at velocities of 37, 24, and $20 \text{ cm } \mu\text{s}^{-1}$ for C, Al, and Cu, respectively, while densities of $1 \times 10^{20} \text{ cm}^{-3}$ expand at 21, 19, and $15 \text{ cm } \mu\text{s}^{-1}$.

Pressure gradients in the radial direction cause the jet to expand laterally. Later in the evolution both simulation and experiments show the development of plasma sidelobes (see Figs. 2 and 3 and Ref. [19]). The sidelobes originate when the jet expands into counterstreaming plasma generated at the sidewalls. A more detailed discussion on the dynamics of the Al jet—which also applies to the C, Cu, and Mo jets studied here—can be found in a previous publication [19]. Below we focus the discussion on the physical mechanisms leading to the increased collimation of jets generated irradiating target materials with higher atomic numbers.

To gain understanding of the role of radiation cooling on jet collimation simulations for an optically thick plasma were compared to simulations that allow for plasma radiation. Figure 4 compares the results of simulations with and without radiation for C, Al, and Cu jets at times when the jets have similar lengths of $\sim 250 \text{ } \mu\text{m}$. Differences in jet collimation at a given time are in large part due to the differences in expansion velocity caused by the differences in mass. Therefore, when comparing the degree of collimation of different jets it is often more meaningful to make the comparison as a function of jet length instead of time. This allows decoupling of the differences in the jet dynamics due to the radiation cooling and other effects from the more trivial difference in expansion velocity due to differences in mass. The optically thick jets generated from materials with different Z ultimately reach similar widths and similar degree of collima-

tion, but the speed at which they evolve depends on the mass. In other words, the degree of collimation of the low and high Z jets is similar, but the latter reach specific length-to-width ratios later in time.

Radiation cooling is observed to have little effect on the C jet, but makes the higher Z jets noticeably more collimated. When compared to the experiment, the simulated optically thick high Z jets in Fig. 4 are noticeably broader. Radiation is computed to reduce the width of the Cu jet by a factor of ~ 5 . This shows that radiation cooling plays a significant role in increasing the collimation of the higher Z jets, which is compatible with the fact that the time-integrated images of the plasma self-emission in Fig. 5 show that the amount of soft-x-ray light emitted from the jet region increases significantly with Z. The increased radiation is the result of the combination of the intrinsically more radiative nature of high Z atoms with the fact that the higher Z jets are denser, which leads to increased electron impact excitation. The higher electron density is associated with the slower expansion velocity of the higher Z materials. A collisional-radiative model computation of the radiation emitted by the different materials using atomic rates obtained with the FLEXIBLE ATOMIC code [29] at the plasma conditions within the jet (ion densities of 1×10^{19} – $1.5 \times 10^{19} \text{ cm}^{-3}$ and electron temperatures of 30–50 eV) shows that a Cu ion radiates two to five times more power than an Al ion and more than 100 times the power of a C ion at the same conditions.

The effect of radiation cooling is quantified by the computed temperature maps shown in Fig. 6. This figure compares the temperature distribution in optically thick (no radiation cooling) C, Al, and Cu jets with those for radiatively cooled jets. The temperature maps correspond to a time of 1 ns after target irradiation, when the jets are fully developed and extend 220–250 μm from the vertex of the groove. The

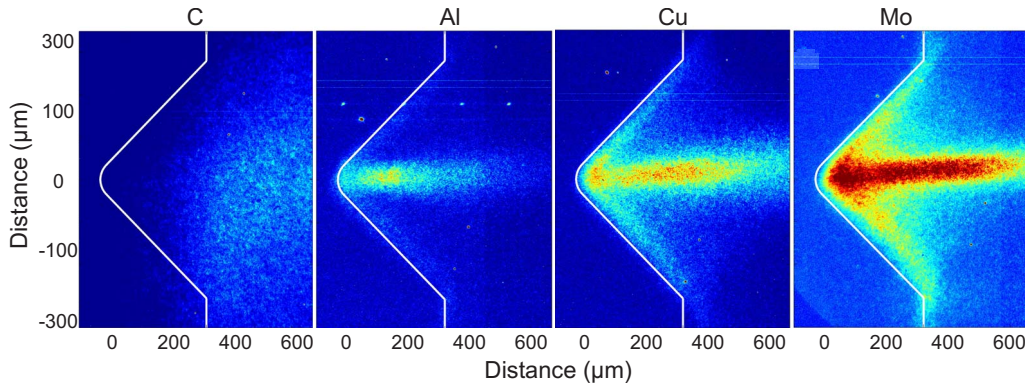


FIG. 5. (Color online) Time-integrated soft-x-ray plasma self-emission images of jets created by laser irradiation of C, Al, Cu, and Mo targets. The amount of radiation emitted by the jet increases with the atomic number of the target material.

electron temperature in the higher Z jets is computed to be drastically reduced by radiation cooling. In the case of Cu the electron temperature at midlength, corresponding to a distance of $\sim 120 \mu\text{m}$ from the vertex, is reduced from 60 to 25 eV.

Figure 7 shows the calculated variation of the radiative cooling rate $1/\tau_{\text{rad}} = q_{\text{rad}}/3/2k(n_e T_e + n_i T_i)$, where q_{rad} is the power density radiated, as the jet evolves reaching different lengths. The jet length is defined here as the distance along the axis measured from the bottom of the groove to the point where the density drops to $1 \times 10^{19} \text{ cm}^{-3}$. The cooling rates were calculated locally and then averaged over the jet volume. Early in the evolution, before the jets have reached a length of $\sim 300 \mu\text{m}$, the Cu jet is computed to have a significantly larger radiation cooling rate than Al and C. As the plasma cools and the jet lengthens, the cooling rate decreases for all three elements. A separate steady-state calculation using a collisionally radiative atomic model computed radiative

cooling rates that were $\sim 2 \times$ lower than the ones obtained in the LTE calculation shown in Fig. 7; nevertheless, the relative cooling rate for the different materials and their dependence was similar. Another way to characterize the degree in which radiation affects the jet dynamics is to compare τ_{rad} to the characteristic hydrodynamic time $\tau_{\text{hydro}} = R_{\text{jet}}/C_s$, where R_{jet} is the radius of the jet taken at half-jet length and C_s is the sound speed. At this position within the jet we find that in the case of carbon $\tau_{\text{rad}} \gg \tau_{\text{hydro}}$, consistent with the fact that the C jet is not significantly affected by radiation. In the case of Al $\tau_{\text{rad}} \sim 2\tau_{\text{hydro}} - 3\tau_{\text{hydro}}$ and Cu $\tau_{\text{rad}} \sim \tau_{\text{hydro}}$, evidence that radiation is important to both of these materials but that the cooling dynamic in Cu occurs at a faster rate.

To identify the role that radiation emitted during the different stages of the plasma evolution has on the observed differences in jet collimation, we compared the experimental results with simulations. Simulations were conducted for (a) no radiation, (b) radiation during only before the jet is

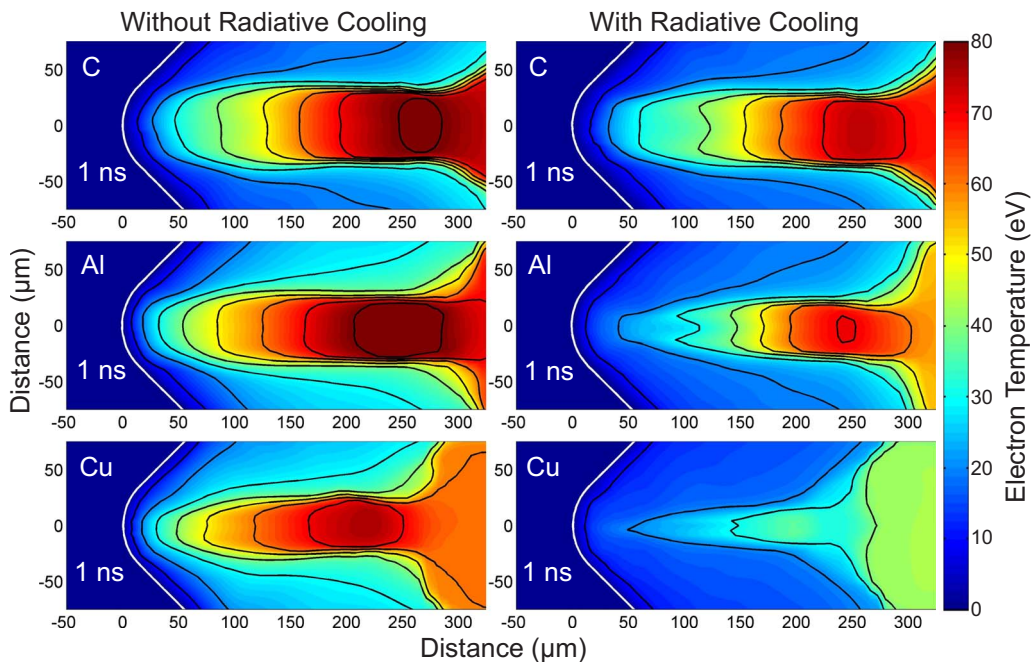


FIG. 6. (Color online) Simulated electron temperature maps for C, Al, and Cu targets at 1 ns into their evolution. Radiation cooling significantly decreases the electron temperature within the higher Z jets.

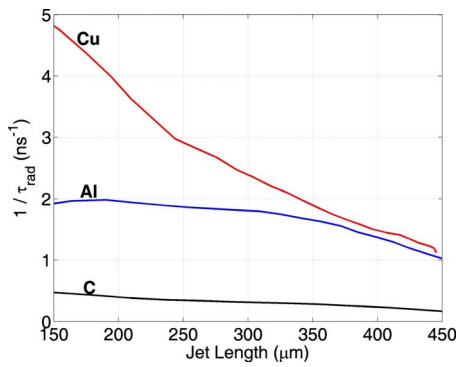


FIG. 7. (Color online) Variation of the radiation cooling rate averaged over the jet volume as the jet evolves reaching different lengths for the C, Al, and Cu plasmas.

formed (plasma turned optically thick after the first 400 ps), and (c) radiation during the entire plasma evolution. Figure 8 compares the measured and computed ratios of the Al to Cu jet widths as a function of jet length. The experimentally determined ratio is shown to reach 2.5 at 270 μm and to monotonically decrease thereafter. The error bar includes both the shot-to-shot experimental variation and the error in measuring the jet width. Without radiation cooling the Al/Cu jet diameter ratio is calculated to remain near unity (~ 1.25) for all jet lengths shown, indicating that the difference in inertial mass of the Al and Cu plasmas does not play a major role in increasing the collimation of the Cu jet. The simulation that only allows for radiation cooling in the formation phase of the jet, when radiation is mostly emitted from within $\sim 50 \mu\text{m}$ of the target surface, also fails to account for the large observed difference in jet collimation. The inclusion of radiation cooling within the jet itself results in a computed Al/Cu jet diameter ratio that is in good qualitative agreement with the experiment. In spite of a moderate quantitative difference possibly related to inaccuracies in computing the copper opacities, the simulation closely resembles the experimentally measured dependence of the jet width ratio as a function of jet length. This result supports the conclusion that radiation cooling significantly enhances the collimation of the higher Z jets.

V. CONCLUSIONS

The collimation of dense plasma jets created by laser irradiation of triangular grooves with low-energy laser pulses

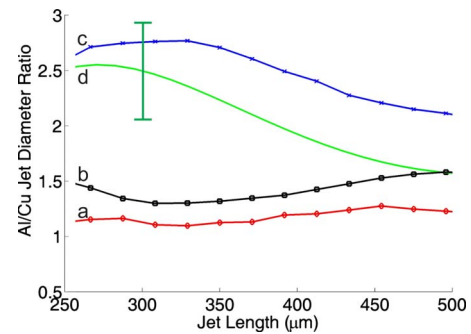


FIG. 8. (Color online) Comparison of measured and simulated ratios of Al to Cu jet widths as a function of jet length. The lines correspond to simulations of optically thick jet (curve a), jet that develops from a plasma that is allowed to radiate during only the first 400 ps of its evolution (curve b), and plasma that radiates during its entire evolution (curve c). The experimental curve (curve d) was obtained using a fit to measure jet width ratios. The error bar represents both the shot-to-shot experimental variation and the error in measuring the jet width.

($\sim 0.6 \text{ J}$) was studied for different materials. The jet density was measured to reach electron densities up to $\sim 1.3 \times 10^{20} \text{ cm}^{-3}$ using soft-x-ray laser interferometry. The jet collimation was measured to increase with Z, reaching a length-to-width ratio of 20 for Mo. In spite of two to three orders of magnitude decrease in the laser pulse energy with respect to previous experiments, radiation cooling is found remain the dominant physical mechanism responsible for the increased collimation of the higher Z jets.

ACKNOWLEDGMENTS

The authors would like to thank M. Marinak and M. Patel for multiple consultations on the use of the code HYDRA. This research was sponsored by the National Nuclear Security Administration under the Stewardship Science Academic Alliances program through U.S. Department of Energy Research Grant No. DE-FG52-06NA26152, using facilities from the NSF ERC Center for Extreme Ultraviolet Science and Technology Award No. EEC-0310717. Part of this work was performed under the auspices of the U.S. Department of Energy by the Lawrence Livermore National Laboratory under Contract No. DE-AC52-07NA27344. The work of M.A.P. was partially supported by ILSA.

-
- [1] R. P. Drake, *High-Energy-Density Physics: Fundamentals, Inertial Fusion, and Experimental Astrophysics (Shock Wave and High Pressure Phenomena)* (Springer Press, New York, 2006).
 [2] B. A. Remington *et al.*, Phys. Plasmas **4**, 1994 (1997).
 [3] B. A. Remington, R. P. Drake, H. Takabe, and D. Arnett, Phys. Plasmas **7**, 1641 (2000).
 [4] D. R. Farley, K. G. Estabrook, S. G. Glendinning, S. H. Glenzer, B. A. Remington, K. Shigemori, J. M. Stone, R. J. Wallace, G. B. Zimmerman, and J. A. Harte, Phys. Rev. Lett. **83**, 1982 (1999).
 [5] K. Shigemori, R. Kodama, D. R. Farley, T. Koase, K. G. Estabrook, B. A. Remington, D. D. Ryutov, Y. Ochi, H. Azechi, J. Stone, and N. Turner, Phys. Rev. E **62**, 8838 (2000).
 [6] J. M. Foster, B. H. Wilde, P. A. Rosen, T. S. Perry, M. Fell, M. J. Edwards, B. F. Lasinski, R. E. Turner, and M. L. Gittings, Phys. Plasmas **9**, 2251 (2002).
 [7] A. Kasperczyk, T. Pisarczyk, J. Badziak, R. Miklaszeski, P. Parys, M. Rosinski, J. Wolowski, C. Stenz, J. Ullschmied, E.

- Krousky, K. Masek, M. Pfeifer, K. Rohlena, J. Skala, and P. Pisarczyk, *Phys. Plasmas* **14**, 102706 (2007).
- [8] A. Kasperczuk, T. Pisarczyk, S. Borodziuk, J. Ullschmied, E. Krousky, K. Masek, M. Pfeifer, K. Rohlena, J. Skala, and H. Hora, *Phys. Plasmas* **13**, 062704 (2006).
- [9] A. Kasperczuk, T. Pisarczyk, S. Borodziuk, J. Ullschmied, E. Krousky, K. Masek, M. Pfeifer, K. Rohlena, J. Skala, and P. Pisarczyk, *Phys. Plasmas* **14**, 032701 (2007).
- [10] P. Nicolai, V. T. Tikhonchuk, A. Kasperczuk, T. Pisarczyk, S. Borodziuk, K. Rohlena, and J. Ullschmied, *Phys. Plasmas* **13**, 062701 (2006).
- [11] S. V. Lebedev, J. P. Chittenden, F. N. Beg, S. N. Bland, A. Ciardi, D. Ampleford, S. Hughes, M. G. Haines, A. Frank, and E. G. B. T. Gardiner, *Astrophys. J.* **564**, 113 (2002).
- [12] D. Ampleford, S. V. Lebedev, S. N. Bland, S. C. Bott, J. P. Chittenden, C. A. Jennings, V. L. Kantsyrev, A. S. Safronova, V. V. Ivanov, D. A. Fedin, P. J. Laca, M. F. Yilmaz, V. Nalajala, I. Shrestha, K. Williamson, G. Osborne, A. Haboub, and A. Ciardi, *Phys. Plasmas* **14**, 102704 (2007).
- [13] R. Kodama, K. A. Tanaka, Y. Sentoku, T. Matsushita, K. Takahashi, H. Fujita, Y. Kitagawa, Y. Kato, T. Yamanaka, and K. Mima, *Phys. Rev. Lett.* **84**, 674 (2000).
- [14] J. M. Stone, N. Turner, K. Estabrook, B. Remington, D. Farley, S. G. Glendinning, and S. Glenzer, *Astrophys. J.* **127**, 497 (2000).
- [15] B. Loupiau, M. Koenig, E. Falize, S. Bouquet, N. Ozaki, A. Benuzzi-Mounaix, T. Vinci, C. Michaut, M. Rabec le Goahec, W. Nazarov, C. Courtois, Y. Aglitskiy, A. Ya. Faenov, and T. Pikuz, *Phys. Rev. Lett.* **99**, 265001 (2007).
- [16] L. B. Da Silva, T. W. Barbee, R. Cauble, P. Celliers, D. Ciarlo, S. Libby, R. A. London, D. Matthews, S. Mrowka, J. C. Moreno, D. Ress, J. E. Trebes, A. S. Wan, and F. Weber, *Phys. Rev. Lett.* **74**, 3991 (1995).
- [17] J. Filevich, K. Kanizay, M. C. Marconi, J. L. A. Chilla, and J. J. Rocca, *Opt. Lett.* **25**, 356 (2000).
- [18] J. Filevich, J. J. Rocca, M. C. Marconi, R. F. Smith, J. Dunn, R. Keenan, J. R. Hunter, S. J. Moon, J. Nilsen, A. Ng, and V. N. Shlyaptsev, *Appl. Opt.* **43**, 3938 (2004).
- [19] J. Grava, M. A. Purvis, J. Filevich, M. Marconi, J. Dunn, S. Moon, and J. Rocca, *Phys. Rev. E* **78**, 016403 (2008).
- [20] C. D. Macchietto, B. R. Benware, and J. J. Rocca, *Opt. Lett.* **24**, 1115 (1999).
- [21] B. R. Benware, C. D. Macchietto, C. H. Moreno, and J. J. Rocca, *Phys. Rev. Lett.* **81**, 5804 (1998).
- [22] Y. Liu, M. Seminario, F. G. Tomasel, C. Chang, J. J. Rocca, and D. T. Attwood, *Phys. Rev. A* **63**, 033802 (2001).
- [23] Y. A. Uspenskii, V. E. Levashov, A. V. Vinogradov, A. I. Fedorenko, V. V. Kondratenko, Y. P. Pershin, E. N. Zubarev, and V. Y. Fedotov, *Opt. Lett.* **23**, 771 (1998).
- [24] M. Purvis, J. Grava, J. Filevich, M. C. Marconi, J. Dunn, S. J. Moon, V. N. Shlyaptsev, E. Jankowska, and J. J. Rocca, *Phys. Rev. E* **76**, 046402 (2007).
- [25] J. Nilsen, J. Castor, C. A. Iglesias, K. T. Cheng, J. Dunn, W. R. Johnson, J. Filevich, M. A. Purvis, J. Grava, and J. J. Rocca, *High Energy Density Phys.* **4**, 107 (2008).
- [26] J. Filevich, J. J. Rocca, M. C. Marconi, S. J. Moon, J. Nilsen, J. H. Scofield, J. Dunn, R. F. Smith, R. Keenan, J. R. Hunter, and V. N. Shlyaptsev, *Phys. Rev. Lett.* **94**, 035005 (2005).
- [27] M. M. Marinak, S. W. Haan, T. R. Dittrich, R. E. Tipton, and G. B. Zimmerman, *Phys. Plasmas* **5**, 1125 (1998).
- [28] M. M. Marinak, G. D. Kerbel, N. A. Gentile, O. Jones, D. Munro, S. Pollaine, T. R. Dittrich, and S. W. Haan, *Phys. Plasmas* **8**, 2275 (2001).
- [29] M. F. Gu, *Astrophys. J.* **582**, 1241 (2003).